IEEE Access
Multidisciplinary | Rapid Review | Open Access Journal

Received 30 June 2022, accepted 11 July 2022, date of publication 15 July 2022, date of current version 22 July 2022.

Digital Object Identifier 10.1109/ACCESS.2022.3191433

RESEARCH ARTICLE

Machine Learning and Prediction of Masked Motors With Different Materials Based on Noise Analysis

PO-JIUN WEN[1,2] AND CHIHPIN HUANG[1]

[1]Institute of Environmental Engineering, National Yang Ming Chiao Tung University, Hsinchu 300093, Taiwan
[2]Radiation and Operation Safety Division, National Synchrotron Radiation Research Center, Hsinchu 300, Taiwan

Corresponding author: Chihpin Huang (huang@nctu.edu.tw)

This work was supported in part by the National Synchrotron Radiation Research Center of Taiwan under Grant 11111SAO01, and in part by the Software Support of PTCOM Technology Company Ltd.

ABSTRACT The effect of noise on the human body has attracted increasing research attention. In particular, many factories generate motor noise pollution, which exposes general workers to noise for extended periods. To solve this problem, masks made of different materials are used for reducing the noise generated by motors. In this study, we attempted to predict the acoustic sound of masked motors. We collected noise level data in decibels for different operation frequencies of motors used at National Synchrotron Radiation Research Center (NSRRC) and developed a machine learning model according to the characteristics of the collected data to simulate the effect of masks on the motor sound. We use the Gradient Boost Model (GBM) as the main learning method because the model is suitable for predicting noise from comparison results of the five models are very common predictive models and may performed as compare method to predict acoustic noise. The results indicated that the prediction accuracy of the GBM was considerably higher than other four traditional machine learning methods (random forests, support vector machine, gaussian processes regression model and multiple linear regression models). Moreover, we used a general multiple linear regression method as the worst method of comparison and conducted time–frequency visualization of the sound for analysis. At NSRRC, we examined the effects of three observation locations and three mask materials, namely wood, metal, and acrylic, on the sound prediction accuracy achieved with the developed model. The highest sound prediction accuracy was obtained behind the motor and under an acrylic mask.

INDEX TERMS Gradient boosting model (GBM), machine learning, motor noise prediction, time–frequency diagrams.

I. INTRODUCTION

Motors are a common source of noise in many noisy working environments. Noise pollution has increased illegal with basic safety practices. The noise and vibration levels of the motor-based machines used in various industries are rising. By reducing the quantity of acoustic energy generated by a motor during operation, the ambient noise can be reduced, thus preventing harm to the physical and mental health of human workers.

Several studies on motor noise have been conducted to improve noise source measurement and prediction. For example, a detailed analysis of the electromagnetic noise generated by an outer rotor permanent magnet motor was reported. The surface vibration of the outer rotor was calculated using the modal analysis method, and the acoustic radiation of the motor was predicted using the acoustic boundary element method [1]. Predicting the acoustic noise distribution of electric motors has emerged as an integral part of the design and control of noise-sensitive applications. To this end, fast and accurate acoustic noise imaging techniques for switched reluctance machines have been developed [2]. According to several researchers, changes in the cogging torque and torque

The associate editor coordinating the review of this manuscript and approving it for publication was Ehab Elsayed Elattar.

ripple parameters of motor deceleration can considerably affect the reduction of vibration and noise. The noise and vibration performance of different motor topologies suitable for electric power steering applications were compared in [3]. To study the electric motor noise and vibration caused by magnetic forces, one should first accurately calculate the stress distribution, which depends on the spatiotemporal distribution of magnetic flux density. Its first discovery lies in a comparison of concentrated force calculation methods including harmonic content, which are the main electromagnetic motor models currently used in vibroacoustic research [4]. A device that can accurately detect engine knock by processing the sound signals captured using high-performance microphones that are sensitive to a wide range of frequencies was developed. The shockwave generated by engine knocking causes the gas in the cylinders of an engine to vibrate, which in turn causes a metallic banging sound to emanate from the outer wall of the engine [5].

Several researchers have employed diverse machine learning techniques to predict noise in various scenarios. For example, in [6], machine learning was used to predict noise and determine the effects of the frequency and intensity of noise on people's psychological states. Satisfactory noise prediction results were obtained in the aforementioned study. In another study, a machine-learning-based method was used to predict the noise level in the surroundings of an F16 fighter jet taking off, and a time–frequency diagram was used for analysis and evaluation to understand the effectiveness of the developed machine learning model in terms of environmental noise prediction [7]. Because the numerical analysis of wind turbine noise levels is extremely challenging and time-consuming, the use of machine learning techniques is preferred for noise estimation [8]. Machine learning models based on backpropagation neural networks have been adopted for determining the noise limit of a vehicle during acceleration by using road history data and for predicting the noise limit in future vehicle noise limit regulations [9]. In road noise research, an effective method for predicting traffic noise levels was developed by considering several aspects, such as the percentage of heavy vehicles, vehicle type, vehicle traffic volume, and average vehicle speed [10]. In particular, to aid data collection, vision-based vehicle detection systems have been developed using machine learning. The traffic noise levels on the Kuwait Ring Road was predicted using the adaptive neuro-fuzzy inference system [11]. The acoustic noise prediction performance of the multiresolution cochleagram model and auditory image model, which are two auditory-based feature extraction models, was compared when they were combined with two supervised machine learning algorithms, namely bag of decision trees and support vector machine [12].

For evaluating acoustic performance by using machine learning, multiple methods that consider time and frequency graph representations of acoustic noise can be used. In [13], a time–frequency graph was used to evaluate the noise suppression performance of a machine learning model. In [14] and [15], a time–frequency graph and correlation matrix were used to explore the influences of various noise sources around the South China Sea, such as ships, warships, plate movements, and wind, on the sound frequency ranges at sea [16]. The time–frequency diagram was used to compare the frequency-domain difference between an original signal and the same signal with various added noise signals. In [17], machine learning was employed to evaluate noise levels by using linear and nonlinear methods in conjunction with several indicators, such as the signal-to-noise ratio. In many studies on noise hazard avoidance and noise prediction, time–frequency maps have been used to evaluate the state of noise [18]. In [19], a time–frequency map of the natural environment was processed using a special filter to analyze and detect different species of birds in nature. Most of these applications rely on calculation of the heart rate and heart rate variability index by using time–frequency or nonlinear domain methods [20]. It mainly studies how to use the technology to ensure that acoustic signal propagation for underwater communication is friendly to sea creatures and does not affect their lives. Moreover, it uses time–frequency diagrams for analysis [21]. In [22], a convolutional neural network (CNN) was used to train a machine learning model by using the time–frequency graph of a human voice as a CNN feature. A mobile application was then developed to detect human speech in real time. Several studies have investigated the identification of the acoustic noise spectra of induction motors by using a frequency-domain, cross-power spectrum estimation algorithm [23]. In these studies, a machine learning model was used for noise simulation, and the prediction results were analyzed using a time–frequency diagram to understand the frequency distribution of noise and the degree of improvement in terms of decibels in different noise states.

Noise improvement can be realized using several approaches. Noise control techniques include sound insulation, sound absorption, vibration reduction, and vibration isolation. To reduce noise, noise barriers, overhanging baffles, and sound-absorbing foam can be installed on sidewalls [24]. According to the law of indestructible mass, low-frequency sound improvement is extremely difficult in engineering because the mass and space of a structure are usually limited. Therefore, a plate-type acoustic metamaterial with a suitable sound insulation effect in the low-frequency range was proposed [25]. Sound insulation performance is a crucial technical index for evaluating the physical performance of building walls. Three structural wood walls integrated using wood-plastic composite were designed to study their sound insulation performance [26]. In the present study, we used acoustic signals and time–frequency diagrams to predict the mask isolation sample and the low-frequency characteristics of the motor for evaluating the designed noise improvement method.

The motor noise in the National Synchrotron Radiation Research Center (NSRRC) facility is distributed in the low-frequency band [27]. In the present study, three materials, namely wood, metal, and acrylic, were used to design

masks for reducing motor noise. Because of the different characteristics, including thickness, structure, size, and motor noise source position, of these masks, many complex variables must be considered to isolate motor noise. The acoustic energy performance of the masks was analyzed and compared. The noise field in this study was created by the simultaneous operation of more than 80 motors. To simulate the noise reduction effect achieved using different masks, the IWATA ISP-500 motor was used in experiments conducted with different masks because the noise sample produced by this motor had a high energy level. Moreover, the acoustic signal strength for the noise insolation effect of the motor masks was simulated using machine learning technology. Next, the noise field was evaluated to identify the most suitable mask material for saving time and reducing costs.

The present study can be divided into three main parts, which are described in the following text:

1. Sound measurement and sampling were performed at different motor positions, and acoustic masks were designed using three materials, namely wood, acrylic, and metal. The sound energy before and after mask use was investigated.

2. The sampled sound frame data and the spectral energy level diagrams of the prepared masks were analyzed. The effects of motor position and mask material on the noise prediction results were investigated.

3. The prediction performance of the machine learning and regression methods were compared.

II. MATERIALS

A. EXPERIMENTAL SETUP

The literature has focused on noise only in terms of the sound energy performance in decibels at different frequencies. In many studies, time–frequency diagrams have been used to explore the distribution of noise energy. Therefore, in the present study, we used time–frequency diagrams to examine the motor noise before and after the application of masks. The source of sound energy was an IWATA ISP-500 motor, and sound was recorded at three locations by using a LAXON high-quality voice recorder, as shown in Fig. 1. The measurement points were located 100 cm above the motor and 50 cm apart from each other. Acoustic signals and sound recordings were obtained from various motor sound data. The recording time at each position was 10 s, and the sampling frequency was 24 000 Hz. Thus, each piece of data contained 240 000 audio points. In experiments, after the motor generated noise, measurements were performed at three positions. Masks made of three materials were then attached to the motor (Fig. 2). For subsequent analyses of the sound produced by the motor with and without the masks,

(a) Recording pen (LAXON)

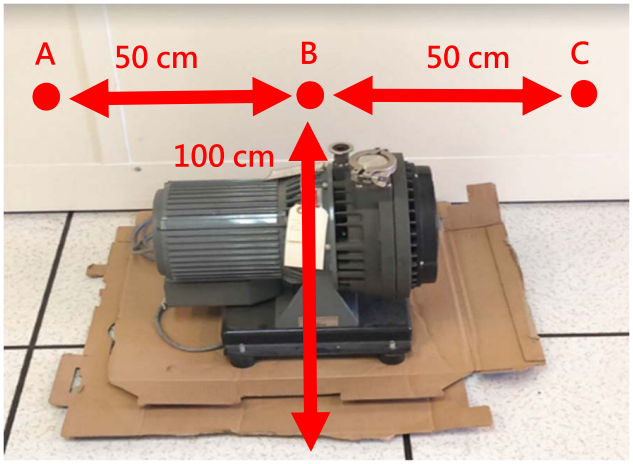

(b) Measurement positions for the motor (IWATA ISP-500) sound

FIGURE 1. Schematic of the recording pen and motor sound measurement positions.

(a) Wood mask

(b) Metal mask

(c) Acrylic mask

FIGURE 2. Schematic of wood mask (a), metal mask (b), and acrylic mask (c).

12 sets of audio files were recorded, and approximately 2 880 000 audio points were generated.

B. EXPERIMENTAL CONCERN

We have make some testing about measure motor mask inside temperature as described below. As shown in Fig. 3, due to the relationship of thermal convection, the motor will generate heat during operation, and there must be enough vertical mask space to discharge hot air. Therefore, the front and rear openings of the fan-mounted mask can have smooth convection, and can also bring the cold air of the working environment air conditioner into the cabin, thereby reducing the heating temperature.

FIGURE 3. Acrylic mask perforates the fan and measures the temperature inside the mask.

As a rule of thumb, the mask can easily cause the motor to overheat. Notably, the material density of the acrylic mask is high, and the heat dissipation effect is the worst among the three materials. Thus, the acrylic mask used in the temperature measurement testing can fully represent the heat dissipation. The test method was to measure the motor temperature before mask and after the inside of the acrylic mask. During 5-50 hours testing results of measuring the inside temperature of the mask found that was 40.7-41.2 °C before the mask and after was 42.3-42.2 °C respectively, so the temperature changes from before and after the mask was only 1-1.6 °C. Therefore, the result of the acrylic mask does not cause drastic changes in temperature, and it is not easy to cause abnormality of the motor.

C. DATA ANALYSIS

In the experiments, 12 sets of 10-s audio files were recorded. Motor sounds were recorded at points A, B, and C [Fig. 1(b)] with and without a mask. The sampling frequency of the recorder was 24 000 Hz; thus, each sound file contained 240 000 amplitude values. These values were stored in the form of a 240 000 $\times 1$ matrix. Before the amplitude matrices were input into the developed machine learning model, the unmasked audio files were sliced into small matrices called

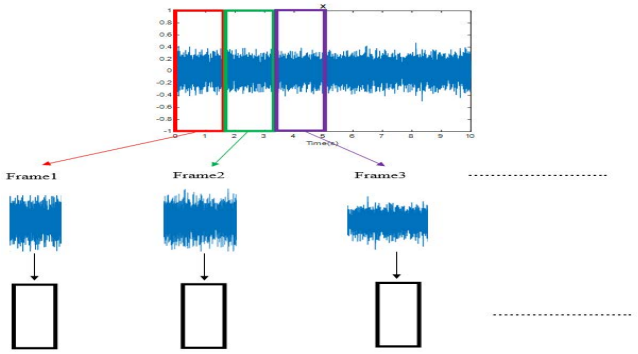

FIGURE 4. Schematic of the slicing of sound into sound frames.

"frames" with a length of N. The frame length was set as 128 in the experiments. A schematic of the slicing process is shown in Fig. 4 [28].

Our purpose was to simulate the motor sound when the motor was covered with a mask. As illustrated in Fig. 5, we used half the input model data as training data and the other half as test data. Consider the sound frame length of 128 as an example. We divided this length into 64 training and 64 testing segments, and each training segment could be predicted. In machine learning, data are generally divided as follows: 80% for training and 20% for testing. However, if sound frames with a length of 128 are subjected to an 80%:20% division, the length of the training and test data would be 102.4 and 25.6, respectively. To ensure that the data lengths are integers and to prevent the lack of data from weakening the effectiveness of training, we used half the data for training and the other half for testing. By stringing together, the results of each predicted sound frame, a complete predicted sound file could be restored, and this file could be compared with the originally recorded sound file.

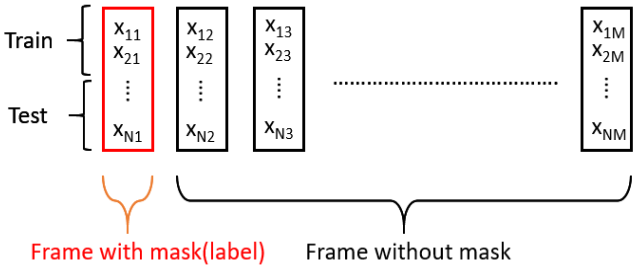

FIGURE 5. Addition of sliced data to the label and division into training and test data.

The simulations of the proposed models were done using MATLAB Version 9.9.0.1592791 2020b. It was executed on a Notebook with an Intel Core-i7-11800H 2.30 GHz processor and 16GB RAM running on 64-bit Windows 10 operating system for fitting gradient boosting model.

III. METHODOLOGY

In [29], In this study, three modeling techniques (gradient boosted machines (GBM), artificial neural networks (ANNs)

and random forests (RF)) were used to compare the performance of local farm-scale calibration with the performance of TN and TC estimates based on local samples selected from two domains added to European datasets. And in [30], the results of PM2.5 predictions in Taiwan demonstrated that the proposed models (long short-term memory, LSTM) outperformed three traditional machine learning methods (gradient boosting, support vector machine, and classification and regression tree models). In another study, evaluating random forest regression (RFR) and multilinearity regression (MLR) methods compared performance. By using RFR, it is possible to determine which explanatory variables affect nitrate contamination in groundwater. Defined RFR and MLR technologies population density is the most important variable explaining reported nitrate contamination [31]. In this paper, tested classifications of brain activity obtained using fMRI during mental imagery in 16 volunteers, in which the number and duration of mental events were not externally imposed but self-generated. To address these issues, we consider two classification techniques (Support Vector Machines, SVM and Gaussian Process, GP), as well as different feature extraction methods. These techniques are combined to determine the procedure that results in the highest precision measurements [32]. In recent years, machine learning has been incorporated into big data analytics due to its great success in learning complex models. Machine learning algorithms such as support vector machines (SVM), random forests (RF), and gaussian processes (GP), etc. have been used to analyze big data to predict a company's financial risk [33]. In [34], we select top-performing companies in 20 industries using the business revenue dataset to predict and model the relationship between features and business revenue by using random forests, gradient boosted regression trees, and support vector machines to solve the revenue forecasting problem of companies. And in [35], the honey industry requires simple, reliable and accurate analysis of honey adulterations to assess their purity for commercial purposes. A comprehensively compare the performance of various machine learning techniques, including the use of linear support vector regression, random forests, gradient boosting and gaussian processes regression, etc. was evaluated. The predictive performance of the above machine learning method is then compared to stacked regression, a technique that integrates the performance of the various techniques described above. Overall [29]–[35], the literature shows that various machine learning techniques can predict other types of targets and compare accuracy levels.

In [36], the random forest gradient was used. The lifting technology model simulates the noise generated by an aircraft wing and air, and it improves the wing shape according to the noise prediction results to reduce flight noise. The air flow around the wing is extremely complex; however, the gradient lifting technology model can yield accurate predictions because it can capture various complex factors. In another study, highway travel times were analyzed and modeled using the gradient boosted regression tree method to improve prediction accuracy and model interpretability. The aforementioned method was compared with another popular method and benchmark models. The results indicated that the gradient boosted model (GBM) has considerable advantages in highway travel time prediction [37].

Moreover, attempts have been made to use the GBM model to predict other types of targets. However, few attempts have been made to use gradient boosting to predict noise. Therefore, the NSRRC designed a model based on the GBM to predict noise, which provides more accurate noise distribution prediction results than multiple linear regression (MLR) [27]. Consequently, in the present study, the GBM was selected as the machine learning model of propose approach for motor noise masking simulation, and random forests (RF), support vector machine (SVM), gaussian processes regression model (GPRM) and multiple linear regression (MLR) were very common prediction models in above literature and may performed as compare method to predict acoustic noise.

However, we will use various criteria to judge the performance of different prediction methods in the literatures. In [38], To analyze the interrelationships between the production prices of rubber, tea and coconut in Sri Lanka, a multivariate time series was used, which also measured the strength of the linear interrelationships between the assets using the *lad-l* cross-correlation matrix (CCM), and selection criteria for AIC, SIC and HQIC fit VAR models. In another study, in order to have a more objective approach and compare the proposed models in a quantitative way to be able to choose the best model among the tentative models, some criteria such as Akaike Information Criterion (AIC), Schwartz Bayesian Information Criterion (SBIC)) and the Hannan-Quinn Information Criterion (HQIC). Applying multiple widely used criteria, the best model was selected for each air pollutant, and the results show that the proposed model performs accurately and satisfactorily in fitting and predicting the fitted and predicted values very close to the relevant true values [39]. In another paper, it provides an empirical study on the causes and socioeconomic impacts of road traffic accidents in Addis Ababa. The optimal number of lags is important for model adequacy and determines the level of statistical significance for explanatory variables and predictions. In this study, alternative techniques to Akaike's Information Criterion (AIC) are presented; Schwarz Bayesian Criterion (BIC), Hannan-Quinn Criterion (HQC), and Log-Likelihood Ratio (LR) [40]. In [41], a seasonal ARIMA (Autoregressive Integral Moving Average) model is used to predict monthly mean sea surface temperature in a time series. Information criteria are often used to measure the goodness of fit of a model. In addition to the information standards BIC, AIC and such as SBIC (Schwartz BIC), AICc (modified version of AIC), HQIC (Hannan-Quinn Information Criteria) as criteria selection model. In another article, we will use the vector autoregressive VAR(P) model in time series to adequately represent the dynamic interactions in the system of variables used for forecasting, which gives ACC, BIC, FPE, SBIC, HQIC the minimum value of and the maximum value of R^2 to predict the ten-year forecast for water supply

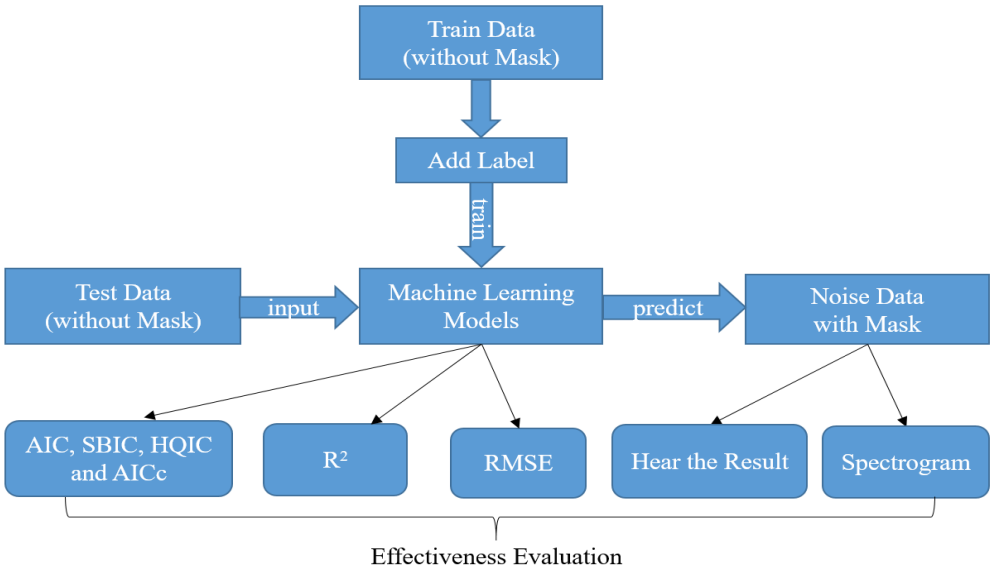

FIGURE 6. Flowchart of the analysis process for experiment.

of Tigris and Euphrates rivers in Iraq [42]. In [43], to this end, the authors propose a multicollinearity-corrected version of the generalized information criterion, which incorporates the effects of multicollinearity and helps statisticians choose the best model among various competing models. The authors also derive the Akaike Information Criterion (AIC), Schwartz Bayesian Criterion (SBIC), Hannan-Quinn Information Criterion (HQIC), Akaike Information Criterion for Small Sample Correction (AICc) by assigning appropriate values to the modified Generalized Information Criterion (MGIC)). In another survey and forecast, food consumption patterns in the Gulf Cooperation Council (GCC) region from 1961 to 2023. Use linear and quadratic forms, Hannan-Quinn (HQIC), Akaike (AIC and AICC), and Schwarz Bayesian (SBIC) information to determine criteria and use their minimum to represent the best model [44].

Therefore, Fig. 6 displays the flowchart of this experiment. After unmasked sound was input into the developed model, the masked sound could be predicted. The learning performance was measured using three group indicators, namely Akaike Information Criterion (AIC), Schwartz Bayesian Criterion (SBIC), Hannan-Quinn Information Criterion (HQIC), Akaike Information Criterion for Small Sample Correction (AICc) and coefficient of determination (R^2), root mean square error (RMSE). The judgment made on the basis of the time–frequency diagram could be directly compared with human hearing.

A. GRADIENT BOOSTING MODEL

The computation performed using Algorithm, namely the GBM process, is described as a flow. The term F(xt) represents the target prediction model. Test samples are input into this model to obtain noise prediction results [27], [29],[30], [34], [35]. Algorithm is presented in the following text.

Algorithm GEM

Input:

1. $F_0(x_t, \beta_0')$
2. $\beta_0 = \arg\min_{\beta_0'} \sum_{i=1}^{N} L(y_{t+24}^i, F_0(x_t^i.\beta'))$
3. M : Iteration times
4. N : Number of data sets

Output: $\mathrm{F}(x_t) = \mathrm{F}_M(\mathrm{x_t})$

5. **For m=l to M**
6. $\mathrm{f_m(x_t)} = -\nabla_{\mathrm{F}} \mathrm{L(y_{l+24}, F_{m-1}(x_t))}$
7. $\beta_m, = \arg\min_{\beta_m'} \sum_{i=1}^{N} \mathrm{L}(yt_{+24}, [\mathrm{F_{m-1}}(x_t^i) + \beta_m'.f_m(x_t^i)])$
8. $F_m(x_t) = F_{m-1}(x_t) + \beta_m.f_m(x_t)$
9. **end**

B. RANDOM FOREST

RF is a non-linear statistical ensemble regression technique that builds a large number of random decision trees and then averages them. There are three core elements in this algorithm, namely the functional model, objective function and optimization algorithm [29], [31], [33]–[35], are represented by the following text.

Algorithm RF

1. $F(x) = \sum_{i=1}^{k} f_i(x; \theta_i)$
2. $E\{F(x)\} = E\{\sum_{i=1}^{k} f_i(x; \theta_i)\}$
3. $\theta_m^{\circ} = argminE\{\sum_{i=1}^{k} f_i(x; \theta_i)\} + f_m(x; \theta_i)$

C. SUPPORT VECTOR MACHINE

SVM is one of the most widespread machine learning algorithms for binary classification. The algorithm has the characteristics of robustness and high accuracy. It is capable of classifying data for almost any problem, including linear and nonlinear problems. The essence of the algorithm is to find

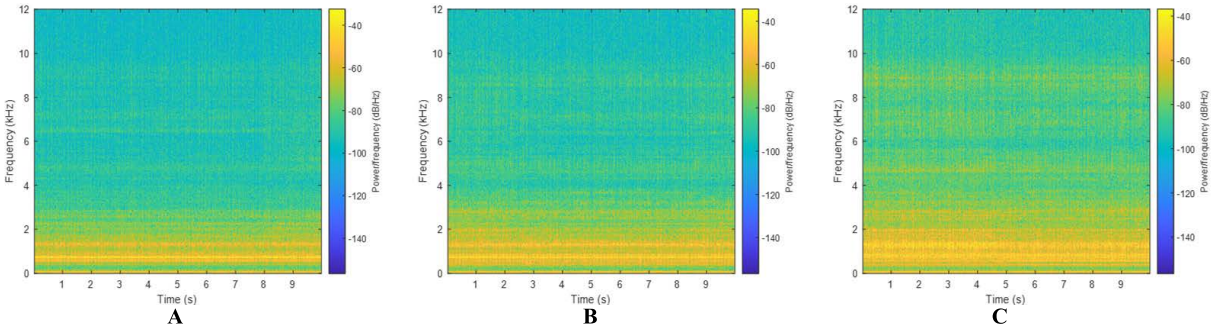

FIGURE 7. Time–frequency diagrams of sound at positions A, B, and C without a mask.

the optimal model with the largest interval [30,32,33,34,35]. Algorithm can be described as the following text.

Algorithm SVM

1. Kernel Function: $K\left(x_i, x_j\right) = \exp\left(-\frac{||xi\text{-}xj||^2}{2\sigma^2}\right)$
2. $y = w^T + b$
3. $w^T + b = k \& w^T + b = -k$
4. $\frac{w}{\|w\|} \cdot (x_+ - x_-) = \frac{w^T(x_+ - x_-)}{\|w\|} = \frac{k}{\|w\|}$

D. GAUSSIAN PROCESSES REGRESSION MODEL

GPRM provides Bayesian methods to establish relationships between input and output variables. For this classification, the expected propagation approximation adopts a posterior pattern, recursively updating the local parameter distribution [32], [35]. The algorithm can be presented in the following text.

Algorithm GPRM

1. data: $D = (x, y) = \left\{(x_i, y_i) \mid i = 1, 2, 3 \ldots\ldots n'\right.$, new input x^*, predict output y^*
2. $K_{\text{matern}}\left(x, x'\right) = \frac{2^{1-v}}{\Gamma(v)}\left(\frac{\sqrt{2v}|d|}{d}\right)^v K_v\left(\frac{\sqrt{2v}|d|}{d}\right)^v, v = 1.50$
3. output $y^* = K\left(x^*, x\right) K(X, X)^{-1} y$
4. $\Gamma(x) = \int_0^\infty t^{z-1} e^{-t} dt$

E. MULTIPLE LINEAR REGRESSION ANALYSIS

In MLR analysis, multiple independent variables are used to predict one dependent variable. Because multidimensional data were used in the conducted experiments, we selected a compound linear regression algorithm that can handle multiple independent variables for prediction [27], [31]. The selected algorithm is presented in the following text.

IV. RESULTS AND DISCUSSION

A. TIME–FREQUENCY DIAGRAM FOR UNMASKED MOTOR NOISE

Fig. 7 displays the energy of the time–frequency signal. The energy of motor sounds with frequencies lower than 2 kHz, that is, low-frequency sounds, is relatively high. Moreover, theenergy of motor sounds with frequencies higher than

Algorithm MLR

1. $y_i = \beta_0 + \beta_1 X_1 + \beta_2 X_2 + \cdots + \beta_p X_{ip} + \epsilon$
2. y_t: dependent variable
3. x i: expanatory variables
4. β_0 : y-intercept(constant term)
5. β_p: slope coefficients for each explanatory variable
6. ϵ: the model's error term(also known as the residuals)

2 kHz gradually decreases. Among the three positions, the highest energy was observed at point C, followed by points B and A. Point C was immediately in front of the motor axis and therefore had a higher sound energy than did the other points. In addition, point A was behind the motor and thus had the lowest sound energy.

B. COMPARISON OF DIFFERENT SIMULATION METHODS

1) SIMULATION DIFFERENT MACHINE LEARNING APPROACHES ANALYSIS FOR THE WOOD MASK

According to various criteria to judge the performance of different machine learning approaches of point A after application of the wood mask, the noise value predicted by GBM, RF, SVM, GPRM and MLR. The best fitted models among the tentative ones along with a number of important measures for selecting the best model are summarized in Table 1. The selected models are shown in bold font in Table 1 in which the best prediction model is selected according to the combined criteria, with (1) minimum AIC, (2) minimum SBIC, (3) minimum HQIC, (4) minimum AICc, (5) maximum R^2 and (6) minimum RMSE. Table 1 is showing the summary of the optimum model selection for the five models based on the selection criteria: AIC of 10.7297, 12.9656, 12.5406, 12.2174 and 14.1127, SBIC of 16.4337, 18.6696, 18.2447, 17.9214, and 22.6688, HQIC of 13.0473, 15.2831, 14.8582, 14.5350 and 17.5891, AICc of 10.8257, 13.0616, 12.6366, 12.3134 and 14.3063, and R^2 of 0.5546, 0.3911, 0.2357, 0.2911 and 0.0236, RMSE of 0.0522, 0.0781, 0.0711, 0.0738 and 0.0629 for GBM, RF, SVM, GPRM and MLR, respectively.

There are a few options to select the best motor noise prediction model from Table 1 depending on which are the information criteria being used. If the values of AIC, SBIC, HQIC, AICc are used, the GBM model is chosen because they

TABLE 1. Different model and different criteria of comparison at point A on the wood mask.

Model	AIC	SBIC	HQIC	AICc	R^2	RMSE
GBM	**10.7297**	**16.4337**	**13.0473**	**10.8257**	**0.5546**	**0.0522**
RF	12.9656	18.6696	15.2831	13.0616	0.3911	0.0781
SVM	12.5406	18.2447	14.8582	12.6366	0.2357	0.0711
GPRM	12.2174	17.9214	14.5350	12.3134	0.2911	0.0738
MLR	14.1127	22.6688	17.5891	14.3063	0.0236	0.0629

are all the lowest values, and the MLR is the worst because it is the highest value. Then, GBM has the highest R^2 and lowest RMSE, so GBM can be determined to be the best model, on the other hand, it has the lowest R^2 value in MLR is the worst model. Therefore, we compared the accuracy of five models using three sets of standard criteria, showing that GBM is the best model and MLR is the worst model, as shown in Table 1.

However, we then more explicitly compared the waveform and sound time-frequency visualization differences between the best model GBM and the worst model MLR to highlight the good performance of GBM prediction. Therefore, considering the above overall arguments and considerations, the best model to consider is the GBM model, and it will be selected and recommended for prediction in this study.

2) SIMULATION WAVEFORM ANALYSIS FOR THE WOOD MASK

According to the waveform of point A after application of the wood mask, the noise value predicted by the GBM [Fig. 8(a)] was close to the actual noise value; however, the noise value predicted through MLR [Fig. 8(b)] did not match the characteristics of the motor sound. In addition, the noise prediction results obtained through MLR were considerably different from the noise in the actual sound files.

3) SIMULATION DIFFERENT ANALYSIS FOR DIFFERENT MASKS

Fig. 9 illustrates the time–frequency diagram for the sound recorded using a voice recorder when the motor was covered with a wood mask. The overall energy at the three points was lower when the motor was covered with the wood mask than when the motor was not masked (Fig. 7). Although the sound energy weakened after the motor was covered with the wood mask, it remained high in the low-frequency region. Figs. 10 and 11 present the simulation results obtained using the GBM and MLR method. These results were close to the measured results. The graphs simulated by the GBM are similar to those depicted in Fig. 9 for low frequencies with high energy and for high frequencies with low energy. However, in the high-frequency regions, a marginal deviation exists relative to the actual value. By contrast, the MLR results were markedly different from the actual values, which indicated that the energy was almost unchanged at all frequencies.

However, as observed when using the metal mask, the overall energy reduction effect achieved using wood was superior to that achieved using metal, and present the simulation results by these two methods were the same as the predicted results for the wood mask.

In addition, the energy reduction effect of wood was superior to that of metal but inferior to that of acrylic, and present

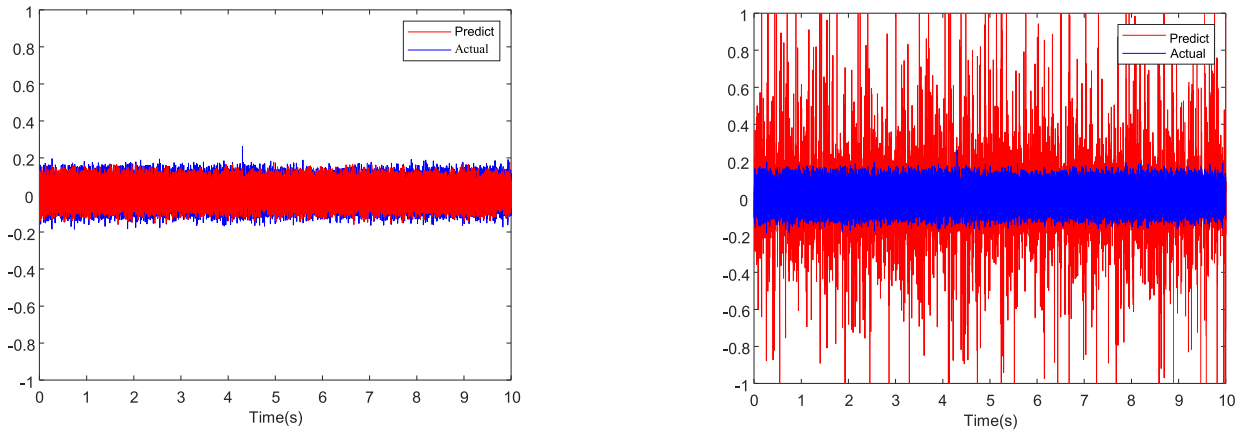

(a) GBM (b) MLR

FIGURE 8. Waveform diagrams comparing the actual sound value at point A on the wood mask with the predictions by using the GBM and MLR.

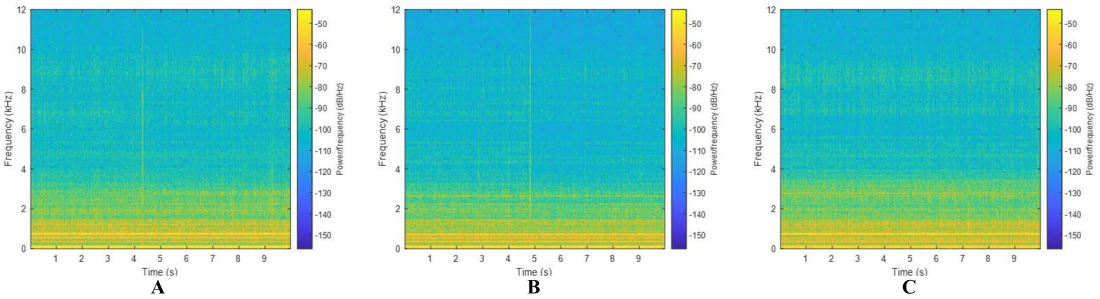

FIGURE 9. Time–frequency diagrams of sound at three positions on the wood mask: A, B, and C.

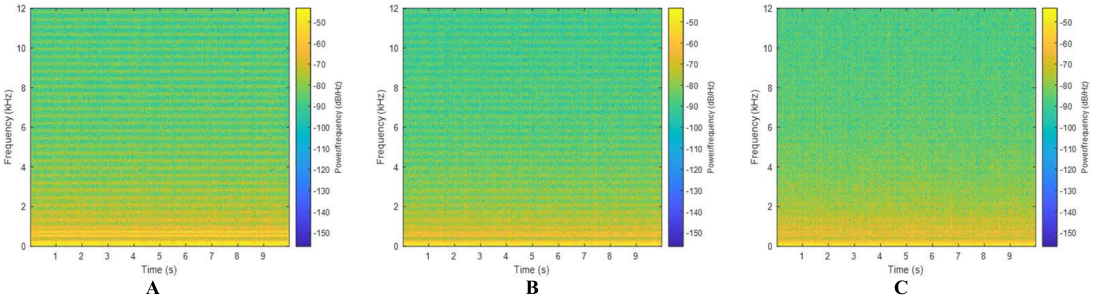

FIGURE 10. Time–frequency diagrams for the predictions of the GBM at three positions on the wood mask: A, B, and C.

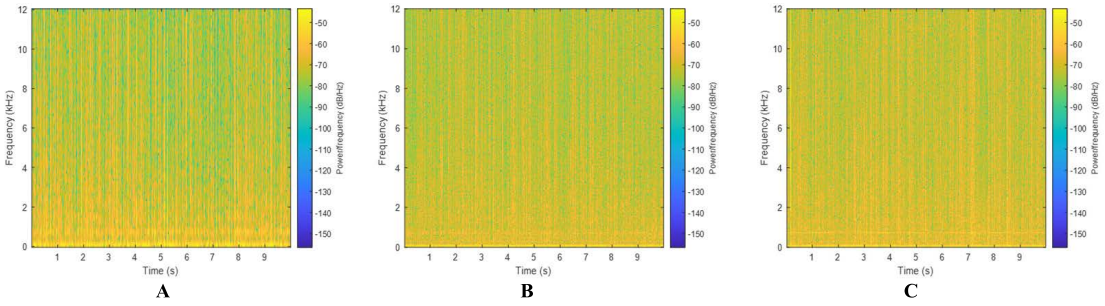

FIGURE 11. Time–frequency diagrams for the MLR simulations at three positions on the wood mask: A, B, and C.

the simulation results were the same as the predicted results for the wood and metal masks.

C. COMPARISON OF DIFFERENT MASKS AND DIFFERENT MEASUREMENT POINTS

According to Table 2, the location with the highest R^2 value differed when different masks were used. Although the R^2 value at point C was extremely stable, it is little change by fluctuate too much with different masks. The average R^2 value for this point was approximately 0.53, which is relatively low. The R^2 values at points A and B fluctuated considerably under the different masks; however, the minimum values did not fluctuate. The difference relative to point C was excessive, and the maximum R^2 value at point C was drastically different.

The average R^2 value at point A was approximately 0.58. The highest average R^2 value was observed at point A, followed by points B ($R^2 = 0.57$) and C ($R^2 = 0.53$). Under the properties of the unmasked sound, the energy at point C was higher than that at points A and B. The sound energy predicted using the GBM model was close to the actual value in the low-frequency region, whereas the predicted value in the high-frequency region deviated considerably from the actual value. However, point C was in front of the motor, and the simulated energy at point C in the high-frequency regions was higher than that at points B and A, which prediction effect is low; thus, the predicted R^2 value was lower than the other two points on average.

TABLE 2. Different masks and different measurement positions for R^2 and RMSE.

MASKS	POSITIONS	R^2	RMSE
WOOD	A	0.5546	0.0522
	B	0.6246	0.0373
	C	0.4841	0.0377
METAL	A	0.4469	0.0279
	B	0.4824	0.0316
	C	0.5496	0.0317
ACRYLIC	A	0.7518	0.0463
	B	0.6178	0.0355
	C	0.5484	0.0341

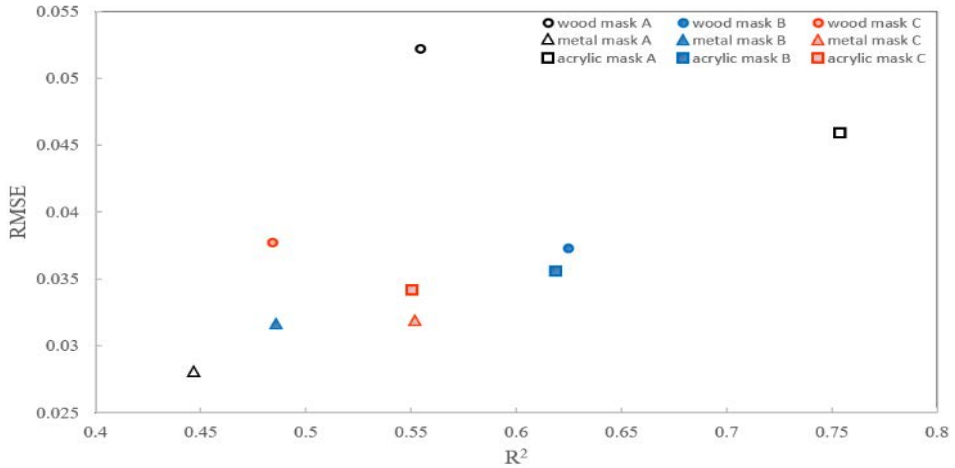

FIGURE 12. Plot of R^2 versus RMSE for the GBM simulations related to the three masks and measurement positions.

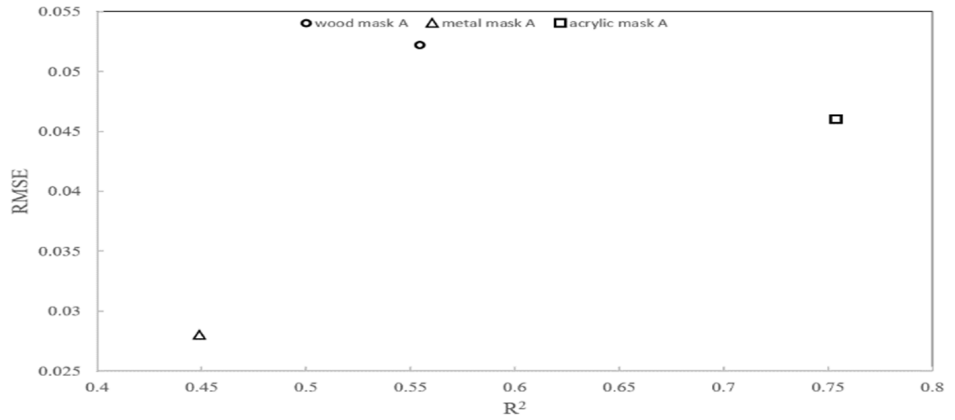

FIGURE 13. Plot of R^2 versus RMSE for the GBM simulations for point A under three masks.

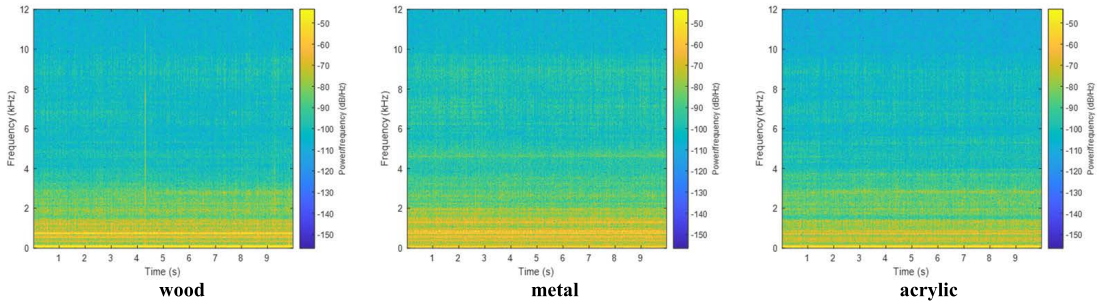

FIGURE 14. Time–frequency diagrams for point A for the three masks.

A comparison of the results obtained for different masks and measurement points indicated that the most accurate predictions were made for the motor being covered with the acrylic mask. The overall trend of the predictions made for the acrylic mask was more accurate than those made for the wood and metal masks, as illustrated in Fig. 12.

D. COMPARISON OF THE PREDICTION FOR DIFFERENT MASKS AT POINT A

According to the obtained results, among the three measurement points, the most accurate predictions were obtained for point A. According to Fig. 13, the most accurate GBM simulations were obtained for the acrylic mask, followed by the wood and metal masks. The RMSE values obtained for the three masks were marginally different. These values were in the range of 0.025-0.055. According to Fig. 14, the order of masks according to the intensity of noise energy after covering the motor was as follows: metal > wood > acrylic. By contrast, according to the results of the GBM illustrated in Fig. 15, the order of masks according to the intensity of noise energy after covering the motor was as follows: acrylic > wood > metal. Therefore, R^2 shows the best simulation

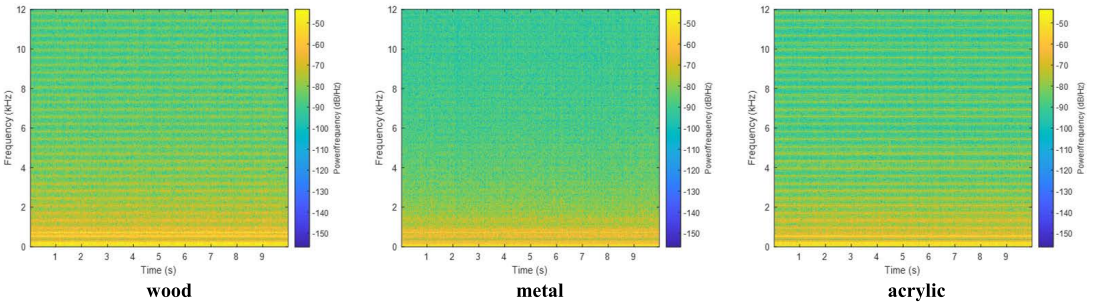

FIGURE 15. Simulated time–frequency diagrams obtained with the GBM for point A for the three masks.

effect of metal mask is poor results are consistent, that the higher sound with high-frequency energy has a worse effect simulated by GBM.

V. CONCLUSION

According to the results of this study, the highest sound prediction accuracy was obtained for a point behind the motor and under the acrylic mask. Moreover, the sound effect predicted by using the GBM model was more accurate than that predicted by using the other four traditional machine learning methods. The simulations of low-frequency sound were well; however, the significant deviation between the predicted energy and the actual energy at high frequencies is a limitation of the developed model. According to the results of the conducted time–frequency analysis, the motor sound corresponded to a low-frequency signal species, that explains the advantages of the proposed approach.

ACKNOWLEDGMENT

The authors would like to thank the staff of the NSRRC in Taiwan.

REFERENCES

[1] S. Zuo, F. Lin, and X. Wu, "Noise analysis, calculation, and reduction of external rotor permanent-magnet synchronous motor," *IEEE Trans. Ind. Electron.*, vol. 62, no. 10, pp. 6204–6212, Oct. 2015.

[2] C. Lin and B. Fahimi, "Prediction of acoustic noise in switched reluctance motor drives," *IEEE Trans. Energy Convers.*, vol. 29, no. 1, pp. 250–258, Mar. 2014.

[3] R. Islam and I. Husain, "Analytical model for predicting noise and vibration in permanent-magnet synchronous motors," *IEEE Trans. Ind. Appl.*, vol. 46, no. 6, pp. 2346–2354, Nov. 2010.

[4] R. Pile, E. Devillers, and J. L. Besnerais, "Comparison of main magnetic force computation methods for noise and vibration assessment in electrical machines," *IEEE Trans. Magn.*, vol. 54, no. 7, Jul. 2018, Art. no. 8104013.

[5] M. Otaka, T. Kasahara, and K. Komaba, "Development of a device that detects knocking by analyzing engine radiation noise," Ono Sokki Co., Ltd., Japan, SAE Tech. Paper 2016-01-1069, Apr. 2016.

[6] H. Zhou, H. Shu, and Y. Song, "Using machine learning to predict noise-induced annoyance," in *Proc. TENCON IEEE Region Conf.*, Jeju, Korea(South), Oct. 2018, pp. 0229–0234.

[7] G. M. Szymański, W. Misztal, M. Orczyk, and P. Komorski, "Modeling of the octave sound spectrum emitted by the F-16 block 52+ aircraft during takeoff," *Measurement*, vol. 170, Jan. 2021, Art. no. 108695.

[8] O. Anicic, D. Petković, and S. Cvetkovic, "Evaluation of wind turbine noise by soft computing methodologies: A comparative study," *Renew. Sustain. Energy Rev.*, vol. 56, pp. 1122–1128, Apr. 2016.

[9] G. Tan, Q. Chen, C. Li, and R. Yang, "A machine learning model for predicting noise limits of motor vehicles in UNECE R51 regulations," *Appl. Sci.*, vol. 10, no. 22, p. 8092, Nov. 2020.

[10] D. Singh, R. Upadhyay, H. S. Pannu, and D. Leray, "Development of an adaptive neuro fuzzy inference system based vehicular traffic noise prediction model," *J. Ambient Intell. Humanized Comput.*, vol. 12, no. 2, pp. 2685–2701, Feb. 2021.

[11] S. AlKheder and R. Almutairi, "Roadway traffic noise modelling in the hot hyper-arid Arabian Gulf region using adaptive neuro-fuzzy interference system," *Transp. Res. D, Transp. Environ.*, vol. 97, Aug. 2021, Art. no. 102917.

[12] S. Abdullah, A. Demosthenous, and I. Yasin, "Comparison of auditory-inspired models using machine-learning for noise classification," in *Proc. Int. J. Simul. Syst., Sci. Technol. Special Issue, Conf. Proc.*, Cambridge, U.K., 2020, pp. 20.1–20.9.

[13] K. Ozawa, M. Morise, S. Sakamoto, and K. Watanabe, "Sound source separation by spectral subtraction based on instantaneous estimation of noise spectrum," in *Proc. 6th Int. Conf. Syst. Informat. (ICSAI)*, Shanghai, China, Nov. 2019, pp. 1137–1142.

[14] J. Zhou, "Analysis of ambient noise spectrum level correlation characteristics in the China sea," *IEEE Access*, vol. 8, pp. 7217–7226, 2020.

[15] L. Xu, K. Yang, and Q. Yang, "Joint time-frequency inversion for seabed properties of ship noise on a vertical line array in South China Sea," *IEEE Access*, vol. 6, pp. 62856–62864, 2018.

[16] S. Ganapathy, "Multivariate autoregressive spectrogram modeling for noisy speech recognition," *IEEE Signal Process. Lett.*, vol. 24, no. 9, pp. 1373–1377, Sep. 2017.

[17] F. J. V. Caballero, D. J. Ives, C. Laperle, D. Charlton, Q. Zhuge, M. O'Sullivan, and S. J. Savory, "Machine learning based linear and nonlinear noise estimation," *J. Opt. Commun. Netw.*, vol. 10, no. 10, pp. D42–D51, Oct. 2018.

[18] M. Yang and A. Wang, "Antinoise performance analysis of spread spectrum system," in *Proc. 2nd Int. Conf. Instrum., Meas., Comput., Commun. Control*, Harbin, China, Dec. 2012, pp. 1443–1447.

[19] N. R. Koluguri, G. N. Meenakshi, and P. K. Ghosh, "Spectrogram enhancement using multiple window savitzky-Golay (MWSG) filter for robust bird sound detection," *IEEE/ACM Trans. Audio, Speech, Language Process.*, vol. 25, no. 6, pp. 1183–1192, Jun. 2017.

[20] D. P. TobóN, S. Jayaraman, and T. H. Falk, "Spectro-temporal electrocardiogram analysis for noise-robust heart rate and heart rate variability measurement," *IEEE J. Transl. Eng. Health Med.*, vol. 5, 2017, Art. no. 1900611.

[21] B. Sherlock, J. A. Neasham, and C. C. Tsimenidis, "Spread-spectrum techniques for bio-friendly underwater acoustic communications," *IEEE Access*, vol. 6, pp. 4506–4520, 2018.

[22] A. Sehgal and N. Kehtarnavaz, "A convolutional neural network smartphone app for real-time voice activity detection," *IEEE Access*, vol. 6, pp. 9017–9026, 2018.

[23] H. Akcay and E. Germen, "Subspace-based identification of acoustic noise spectra in induction motors," *IEEE Trans. Energy Convers.*, vol. 30, no. 1, pp. 32–40, Mar. 2015.

[24] M. J. Owoyemi, B. C. Falemara, and A. J. Owoyemi, "Noise pollution and control in wood mechanical processing wood industries," *Biomed. Statis. Informat.*, vol. 2, no. 2, pp. 54–60, Jun. 2017.

[25] X. Zhou, L. Wang, L. Qin, and F. Peng, "Improving sound insulation in low frequencies by multiple band-gaps in plate-type acoustic metamaterials," *J. Phys. Chem. Solids*, vol. 146, Nov. 2020, Art. no. 109606.

[26] X. Yang, X. Tang, L. Ma, and Y. Sun, "Sound insulation performance of structural wood wall integrated with wood plastic composite," *J. Bioresour. Bioproducts*, vol. 4, no. 2, pp. 111–118, May 2019.

[27] P.-J. Wen and C. Huang, "Noise prediction using machine learning with measurements analysis," *Appl. Sci.*, vol. 10, no. 18, p. 6619, Sep. 2020.
[28] S.-H. Fang, Y. Tsao, M.-J. Hsiao, J.-Y. Chen, Y.-H. Lai, F.-C. Lin, and C.-T. Wang, "Detection of pathological voice using cepstrum vectors: A deep learning approach," *J. Voice*, vol. 33, no. 5, pp. 634–641, Sep. 2019.
[29] S. Nawar and A. M. Mouazen, "Comparison between random forests, artificial neural networks and gradient boosted machines methods of on-line vis-NIR spectroscopy measurements of soil total nitrogen and total carbon," *Sensors*, vol. 17, no. 10, p. 2428, 2017.
[30] L. Lin, C.-Y. Chen, H.-Y. Yang, Z. Xu, and S.-H. Fang, "Dynamic system approach for improved $PM_{2.5}$ prediction in Taiwan," *IEEE Access*, vol. 8, pp. 210910–210921, 2020.
[31] I. Ouedraogo, P. Defourny, and M. Vanclooster, "Application of random forest regression and comparison of its performance to multiple linear regression in modeling groundwater nitrate concentration at the African continent scale," *Hydrogeology J.*, vol. 27, no. 3, pp. 1081–1098, Dec. 2018.
[32] J. Schrouff, C. Kussé, L. Wehenkel, P. Maquet, and C. Phillips, "Decoding semi-constrained brain activity from fMRI using support vector machines and Gaussian processes," *PLoS ONE*, vol. 7, no. 4, Apr. 2012, Art. no. e35860.
[33] G. Teles, J. J. Rodrigues, R. A. Rabêlo, and S. A. Kozlov, "Comparative study of support vector machines and random forests machine learning algorithms on credit operation," *Softw., Pract. Exper.*, vol. 51, no. 12, pp. 2492–2500, Dec. 2021.
[34] H. Lei and H. Cailan, "Comparison of multiple machine learning models based on enterprise revenue forecasting," in *Proc. Asia–Pacific Conf. Commun. Technol. Comput. Sci. (ACCTCS)*, Shenyang, China, Jan. 2021, pp. 354–359.
[35] G. G. Dumancas and H. Ellis, "Comprehensive examination and comparison of machine learning techniques for the quantitative determination of adulterants in honey using Fourier infrared spectroscopy with attenuated total reflectance accessory," *Spectrochim. Acta A, Mol. Biomol. Spectrosc.*, vol. 276, Aug. 2022, Art. no. 121186.
[36] A. Patri and Y. Patnaik, "Random forest and stochastic gradient tree boosting based approach for the prediction of airfoil self-noise," *Proc. Comput. Sci.*, vol. 46, pp. 109–121, Apr. 2015.
[37] Y. Zhang and A. Haghani, "A gradient boosting method to improve travel time prediction," *Transp. Res. C, Emerg. Technol.*, vol. 58, pp. 308–324, Sep. 2015.
[38] K. A. Nyantakyi, B. L. Peiris, and L. H. P. Gunaratne, "Analysis of the interrelationships between the prices of Sri Lankan rubber, tea and coconut production using multivariate time series," *Adv. Econ. Bus.*, vol. 3, no. 2, pp. 50–56, Feb. 2015.
[39] J. Delaram and M. Khedmati, "Forecasting ambient air pollutants by box-Jenkins stochastic models in Tehran," *Scientia Iranica, Trans. E, Ind. Eng.*, vol. 28, no. 6, pp. 3551–3568, Dec. 2021.
[40] T. G. Bekele and T. H. Sima, "Road traffic accident cause and effect on socio economy of Addis Ababa city," *Econ. Social Sci. Academic J.*, vol. 1, no. 4, pp. 21–37, 2019.
[41] C. C. Wong and J. Kishigami, "Time series forecast of sea surface temperature for Hokkaido fishery ports along coastal line of Japan sea," in *Proc. Int. Conf. Ind. Eng. Oper. Manag.*, Johannesburg, South Arica, Oct. 2018, pp. 1398–1408.
[42] M. A. M. Badal, "Using multivariate time series model VAR(P) to forecast water supply of tigris and Euphrates rivers in Iraq," *J. Humanity Sci.*, vol. 22, no. 6, pp. 220–228, Dec. 2018.
[43] D. S. Jayakumar and A. Sulthan, "Identification of multicollinearity and it's effect in model selection," *Electron. J. Appl. Stat. Anal.*, vol. 7, no. 1, pp. 153–179, Apr. 2014.
[44] O. E. Elsheikh, M. M. Alderiny, and S. H. A. Alkahtani, "Food transition in the Gulf cooperation council region," *Afr. J. Agricult. Res.*, vol. 15, no. 2, pp. 297–311, Feb. 2020.

PO-JIUN WEN is currently pursuing the Ph.D. degree with the Institute of Environmental Engineering, National Yang Ming Chiao Tung University, Hsinchu, Taiwan. His current research interests include the noise monitoring IoT, machine learning, and environmental measurement techniques.

CHIHPIN HUANG received the Ph.D. degree from the Department of Environmental Engineering, Delaware University, USA. He is currently the Lifelong Chair Professor with the Institute of Environmental Engineering, and the Director of Environmental Technology and Smart Research, ETSS, University of National Yang Ming Chiao Tung, Hsinchu, Taiwan. He has authored or coauthored over 180 journal articles, conference papers, patents, and editorials in his research areas. His research interests include the use of the IoT and machine learning techniques for optimal design and operational control of wastewater treatment and noise monitoring. He is a fellow of International Honorary Member, The American Academy of Environmental Engineers and Scientists (AAEES).